Applied Catalysis B: Environmental 84 (2008) 552–562

Contents lists available at ScienceDirect

Applied Catalysis B: Environmental

journal homepage: www.elsevier.com/locate/apcatb

The effects of La_2O_3 on the structural properties of La_2O_3–Al_2O_3 prepared by the sol–gel method and on the catalytic performance of Pt/La_2O_3–Al_2O_3 towards steam reforming and partial oxidation of methane

J.C.S. Araujo [a], D. Zanchet [b], R. Rinaldi [c], U. Schuchardt [c], C.E. Hori [d], J.L.G. Fierro [e], J.M.C. Bueno [a,*]

[a] Departament of Chemical Engineering, Universidade Federal de São Carlos, C.P. 676, 13565-905 São Carlos, SP, Brazil
[b] Laboratório Nacional de Luz Síncrotron, LNLS, C.P. 6192, 13083-970 Campinas, SP, Brazil
[c] Institute of Chemistry, Universidade Estadual de Campinas, 13083-970 Campinas, SP, Brazil
[d] FEQ, Universidade Federal de Uberlândia, Av. Joao Naves de Ávila 2121, Campus Santa Monica, Bloco 1K, 38400-902 Uberlândia, MG, Brazil
[e] Institute of Catalysis and Petrochemistry, CSIC, Cantoblanco, 28049 Madrid, Spain

ARTICLE INFO

Article history:
Received 22 February 2008
Received in revised form 12 May 2008
Accepted 16 May 2008
Available online 24 May 2008

Keywords:
Sol–gel
Lanthanum oxide
Platinum on alumina
CO adsorption
Steam reforming of methane
Partial oxidation of methane

ABSTRACT

The effect of La_2O_3 content on the structural properties and catalytic behavior of Pt/xLa_2O_3–Al_2O_3 catalysts in steam reforming of methane and partial oxidation of methane was investigated. There was a decrease in the density of Pt sites with the increase of La_2O_3 loadings according to Fourier transform infrared spectroscopy of adsorbed CO and to dehydrogenation of cyclohexane results. However, transmission electron microscopy data indicates an opposite trend. This apparent disagreement could be due to the partial coverage of Pt sites by LaO_x species. CH_4 turnover rates and specific rates of steam reforming of methane increased for higher La_2O_3 loadings. The Pt/Al_2O_3 catalyst was strongly deactivated during partial oxidation of methane, while La_2O_3-containing catalysts exhibited higher stability. The increase of activity observed during the reactions was ascribed to the ability of the $[LaPt_xO]Pt^0$-like species to promote the gasification of coke. This cleaning mechanism led to higher accessibility of the active sites to CH_4.

1. Introduction

Processes to transform natural gas into hydrogen or synthesis gas have been extensively studied in recent decades. Hydrogen can be used in fuel cells as a power source and syngas may be converted into hydrocarbons via the Fischer–Tropsch synthesis. Increase of environmental restrictions forcing the reduction of exhaust emissions and interest in diminishing dependence on petroleum, associated to the continuous increase of probed natural gas reserves, are factors that justify the great deal of attention given to methane reforming processes.

Partial oxidation and autothermal reforming of methane present some advantages relative to steam reforming, since they are able to produce streams with different H_2/CO ratios. In addition, the high energy required by reforming reactions can be generated *in situ* through coupled-oxidation reactions, helping to reduce the effective production costs. However, thermodynamic properties of methane reforming reactions still require elevated temperatures (~1073 K) to obtain high methane conversions. Another common problem is carbon formation on the catalyst surface. The combination of high temperature, presence of oxygen and susceptibility to carbon deposition requires catalysts with particular properties, such as resistance to carbon deposition and stability against sintering of the highly dispersed metal phase. A number of reports have shown that methane can be activated on metal surfaces (Ni, Rh, Pt, Ir and Ru), and that higher metal dispersions favor methane reforming reactions [1,2]. In an earlier work [3], we demonstrated that $Pd/CeO_2/Al_2O_3$ promoted with high ceria loading showed higher activity for steam reforming of methane. This fact was attributed to an increase of the accessibility of CH_4 to active metal sites for oxygen transfer from ceria to the Pd surface, providing a carbon-removing route. For the $Pt/CeO_2/Al_2O_3$ system, the addition of higher ceria loadings led to better catalytic activity and stability for partial oxidation of methane due to the formation of a larger Pt–CeO_2 interface [4]. Nagai et al. [5] reported that the interaction between PtO and the support may act as an anchor, inhibiting the sintering of Pt particles on ceria-based oxide.

* Corresponding author. Tel.: +55 16 33518439; fax: +55 16 33518466.
E-mail address: jmcb@ufscar.br (J.M.C. Bueno).

0926-3373/$ – see front matter © 2008 Elsevier B.V. All rights reserved.
doi:10.1016/j.apcatb.2008.05.011

Although previous reports had revealed that ceria can be an important component of methane reforming catalysts, several studies have also demonstrated that noble metals supported on lanthana exhibit high activity and stability [6–8]. La_2O_3 is described as a better promoter than ceria to stabilize transitional aluminas [9]. In addition, it is also able to stabilize Pt dispersion. These properties suggest that La_2O_3 supported on alumina could be a system of considerable interest for methane reforming.

The sol–gel method to prepare metal-supported catalysts has been demonstrated to be useful for a large number of industrial applications [10–16]. Sol–gel processes result in materials with high surface area, high porosity in the mesoporous range and good thermal stability [11,12,17,18], as reported for La_2O_3–Al_2O_3 mixed oxides [9,19].

Considering these aspects, the present work is a continuation of the study of CeO_2/Al_2O_3 supported Pt, Pd catalysts using lanthana instead of ceria [3,4,20]. The current work aims to address: (i), the effect of La_2O_3 content on the structural properties of La_2O_3–Al_2O_3 supports obtained by the sol–gel method; (ii), the effect of La_2O_3 content on the superficial Pt structure; and (iii), the effect of the properties of Pt/La_2O_3–Al_2O_3 catalysts on activity for steam reforming of methane and stability for partial oxidation of methane. A combination of techniques such as N_2 adsorption, X-ray diffraction (XRD), thermogravimetric analysis (TGA), differential thermogravimetric analysis (DTA), temperature-programmed reduction (TPR), ^{27}Al NMR spectroscopy (^{27}Al MAS NMR), X-ray photoelectron spectroscopy (XPS), Fourier transform infrared spectroscopy (FTIR) of CO adsorption and transmission electron microscopy (TEM) was used in the characterization of xerogels, supports and catalysts.

2. Experimental

2.1. Synthesis of Pt/xLa_2O_3–Al_2O_3 catalysts

Precursors of xLa_2O_3–Al_2O_3 mixed oxides, where x is the lanthana content (wt.%), were prepared by the sol–gel method [21]. Typically, a solution of $La(NO_3)_3{\cdot}6H_2O$ (99.9%, Aldrich), containing appropriate amounts of La(III) to obtain xLa_2O_3–Al_2O_3 xerogels ranging from 1 to 20 wt.% of La_2O_3, was added to a slurry containing 103.5 mmol of aluminum tri-*sec*-butoxide (Al(O-*s*Bu)$_3$, p.a., 99%, Merck) and 3.25 mol of absolute ethanol (Merck 99.5%). The molar ratio of H_2O/alkoxide was 23.5 for all syntheses. The slurry was kept under vigorous stirring at 373 K and refluxed for 1 h. In sequence, 25 mL of a 0.10-mol L^{-1} nitric acid solution was added to the slurry for peptization. The slurry was refluxed for an additional 14 h. After this, the gels were dried for 2–3 days under air at room temperature. The resulting xerogels were calcined at 1223 K for 6 h under a flow of synthetic air, yielding a series of xLa_2O_3–Al_2O_3 mixed oxides, which were used as supports for Pt/xLa_2O_3–Al_2O_3 catalysts.

Pt/xLa_2O_3–Al_2O_3 catalysts were obtained by impregnation of xLa_2O_3–Al_2O_3 supports using an ethanolic solution of $H_2PtCl_6{\cdot}6H_2O$ (Umicore Brasil). The mixture was stirred for 4 h at room temperature and kept for 1 h at 328 K. Finally, the ethanol was removed using a rotary evaporator at 343 K. The solids were maintained at 333 K overnight and calcined at 573 K under a flow of synthetic air for 2 h. For all samples, the amount of Pt was 0.5 wt.%. These supports and catalysts are referred to as *x*LA and Pt/*x*LA, respectively, where x is wt.% of La_2O_3.

2.2. Characterization

Chemical analyses of the catalysts were performed by inductively coupled plasma-atomic emission spectroscopy (ICP) on a PerkinElmer Optima 3300 DV device. The composition of the samples is summarized in Table 1.

Surface area (S_{BET}) and pore volume (V_p) of *x*LA supports and Pt/*x*LA catalysts were measured by N_2 adsorption–desorption isotherms at 77 K using a Micromeritics ASAP 2000 apparatus. The samples were degassed at 473 K under vacuum for 2 h. BET surface area (S_{BET}) and average pore size diameter (D_p) were calculated using the BET and BJH methods, respectively.

XRD patterns were collected with a Rigaku Multiflex diffractometer using Cu Kα radiation. The step-scans were taken over the range of 2θ from 5° to 80° with step-sizes of 0.02° and counting times of 2 s. The apparent crystallite sizes of xerogels were determined by Scherrer's equation using the (0 2 0) reflection of boehmite [13].

TPR of the catalysts was carried out using a Micromeritics Pulse Chemisorb 2705 instrument fitted with a thermo conductivity detector (TCD). Prior to reduction experiments, the samples (0.100 g) were pretreated at 423 K in a N_2 stream for 1 h. After cooling to room temperature, the catalysts were heated to 1273 K at a rate of 10 K min^{-1} in a flow of 5% H_2/Ar (50 mL min^{-1}) while the TCD signal was recorded. In order to remove water from the exit stream the effluent gas was passed through a cold trap filled with a mixture of propanol–liquid nitrogen before the TCD. Temperature-programmed desorption of H_2 (TPD-H_2) was carried out in the same equipment, with H_2 adsorption occurring at 298 K. The Pt dispersion of Pt/Al_2O_3 catalysts was calculated from the H_2 desorbed from the Pt surface during the heating.

FTIR of adsorbed CO were recorded using a Thermo Nicolet 4700 Nexus FT-IR spectrophotometer with MCT detector and diffuse reflectance infrared Fourier transform Spectroscopy-reactor cell (Spectra Tech) with CaF_2 windows (DRIFT HTHV cell). IR spectra were recorded using 64 scans at 4 cm^{-1} resolution. The catalysts were reduced at 923 K under a 25% H_2/N_2 mixture for 2 h. The

Table 1
Chemical analysis of Pt/*x*LA samples, textural properties of *x*LA xerogels, supports and catalysts and apparent crystallite sizes ($L_{boehmite}$) of boehmite

Pt (wt.%)	$x_{nominal}$ La_2O_3 (wt.%)	x_{real} La_2O_3 (wt.%)	*x*LA xerogels[a]				*x*LA supports[b]			Pt*x*LA catalysts[c]		
			S_{BET} (m^2/g)	V_p (cm^3/g)	D_p (nm)	$L_{boehmite}$ (nm)	S_{BET} (m^2/g)	V_p (cm^3/g)	D_p (nm)	S_{BET} (m^2/g)	V_p (cm^3/g)	D_p (nm)
0.49	0	0	248	0.23	3.7	2.4	325	0.45	9.6	215	0.25	4.4
0.48	1	0.9	276	0.26	3.8	1.7	191	0.28	2.9	142	0.23	3.3
0.51	3	2.9	288	0.24	3.3	1.5	190	0.28	2.0	148	0.22	2.5
0.48	6	5.8	253	0.19	3.1	1.2	200	0.29	1.9	150	0.22	2.2
0.49	12	11.8	164	0.10	2.6	1.1	191	0.17	1.8	119	0.15	2.2
0.49	20	19.9	86	0.05	2.6	1.0	190	0.15	1.9	110	0.12	2.1
0.48	100	–	–	–	–	–	–	–	–	–	–	–

[a] *x*LA xerogels dried at room temperature.
[b] *x*LA supports calcined at 1223 K.
[c] Pt/*x*LA catalysts calcined at 573 K.

adsorption of CO was performed at room temperature with CO pulses (0.5 mL) at a CO pressure of 20 Torr. Each spectrum was collected after 5 min in order to achieve equilibrium. Temperature-programmed desorption of CO (TPD-CO) experiments were carried out according to Ref. [3].

X-ray photoemission spectra were obtained with a VG ESCALAB 200R spectrometer equipped with a hemispherical electron analyzer and an Al Kα ($h\nu$ = 1486.6 eV, 1 eV = 1.6302×10^{-19} J) 120 W X-ray source. Powdered samples were pressed into an aluminium block mounted on a sample rod placed in a pre-treatment chamber and heated under vacuum at 373 K for 1 h. After this, the sample was transferred to the analysis chamber. The residual pressure inside the analysis chamber was below 1.0×10^{-8} mbar. Binding energies (BE) of O 1s, Al 2p, La 3d and Pt 4d were determined by fitting the measured spectra and referred to the C 1s line at 284.8 eV. These fits were done using the XPSpeak® software. The curves obtained were a mixture with different proportions of Lorentzian and Gaussian functions. Pt/La and Pt/Al surface atomic ratios were calculated using the area of the peaks corresponding to Al 2p, La 3d and Pt 4d.

TGA and DTG of *x*LA xerogels were obtained using a TA Micrometrics 2050 TGA instrument. The samples were heated from room temperature up to 1473 K (10 K min^{-1}) under a flow of synthetic air of 100 mL min^{-1}.

^{27}Al MAS NMR spectra were recorded for xerogels, *x*LA supports and Pt/*x*LA catalysts using a Varian INOVA 500 MHz spectrometer, operating at 130.26 MHz and equipped with a 4-mm high-speed magic-angle spinning probe (Doty Scientific Inc.) at a spinning rate of 13 kHz. ^{27}Al chemical shifts are referenced to a 1.0-mol L^{-1} $Al(NO_3)_3$ solution. The experimental conditions were acquisition time of 5 ms, pulse width of 2.4 μs ($\pi/2$), recycle delay of 0.1 s and spectral width of 32.2 kHz. For each spectrum, 2400 scans were acquired. FIDs were processed using an exponential function with a line width of 1 Hz. The spectra were fitted using the OriginPro 7.5® program (OriginLab Corporation).

High-resolution TEM images were obtained in a JEOL JEM-3010 microscope (300 kV, 1.7 Å point resolution) at the Brazilian Synchrotron Light Laboratory, Campinas, SP, Brazil. TEM samples were prepared by dropping a suspension containing the catalyst previously reduced at 923 K in isopropanol onto amorphous carbon films supported on copper grids.

2.3. Catalytic reactions

2.3.1. Dehydrogenation of cyclohexane reaction

Pt dispersion was determined from the rate of dehydrogenation of cyclohexane, a structure insensitive reaction [22], and compared with a standard sample. The reaction was performed in a fixed-bed reactor at atmospheric pressure using catalyst powders (10 mg; 80–100 mesh particles). The samples were reduced at 923 K under a H_2 flow at 30 mL min^{-1} and the reaction was carried out at 543 K with space velocity (WHSV) of 170 h^{-1}. The reactants were fed to the reactor by bubbling H_2 through a saturator containing cyclohexane at 285 K (H_2/HC = 13.6). Effluent gas compositions were analyzed by gas chromatography (HP5890) using with a HP-INNOWAX capillary column.

2.3.2. Steam reforming of methane

Rates for steam reforming of CH_4 were measured in a fixed bed quartz reactor (i.d. 8 mm) and with a type K thermocouple enclosed within a sheath in contact with the catalyst bed. The reactions were carried out under atmospheric pressure using catalyst powders (100 mg; 80–100 mesh particles) diluted with quartz beads (300 mg) of similar granulometry. Samples were reduced to 923 K under a H_2 flow at 30 mL min^{-1}. Effluent gas compositions were analyzed by gas chromatography, employing a combination of two GCs (Varian-3400) having a TCD detector. For reaction product analysis, two columns of Porapak N and Molecular Sieve 13× were used in a series-bypass arrangement. The feed composition ratio of CH_4:H_2O:N_2 was 1:3:0.4 at a total flow rate of 2×10^{-2} mol min^{-1}. CH_4 turnover frequency (TOF_{CH_4}) at zero conversion was calculated from plotting the reaction rate versus methane conversion, in a range of CH_4 conversion from 1 to 13%. Apparent activation energies (E_a^{app}) were estimated using non-linear methods to fit experimental data to the Arrhenius equation. Pt dispersion was obtained from the dehydrogenation of cyclohexane reaction.

2.3.3. Partial oxidation of methane

Partial oxidation of methane was carried out in a fixed bed quartz reactor at atmospheric pressure. Each test used 40 mg of sample diluted in SiC (72 mg). Before the reaction, the catalyst was heated at 423 K under a N_2 flow at 30 mL min^{-1}, for 0.5 h. After this, the reduction was done at 923 K under H_2 flow at 30 mL min^{-1}, for 2 h. Then, the reduced sample was heated to 1073 K under N_2 flow. For the reaction, a mixture of CH_4:O_2:N_2 with molar ratios of 2:1:0.9 was passed through the reactor at 130 mL min^{-1} and WHSV = 80 h^{-1}. The reaction products were analyzed as described in the previous section.

3. Results

3.1. Chemical analysis

Chemical analyses of Pt/*x*LA samples are summarized in Table 1. The results demonstrate that La and Pt contents are close to nominal values.

3.2. X-ray powder diffraction

XRD patterns of *x*LA xerogels (*x* = 0–20 wt.% of La_2O_3) correspond to a pseudo-boehmite structure [23] (Fig. 1A). Pseudo-boehmite apparent crystallite sizes (Table 1), estimated using the Scherrer's equation, decreased with the increase of La_2O_3 content. It is important to recall that part of the decreased intensities of boehmite reflections can be attributed to greater absorption of X-rays by La atoms (compared to Al atoms).

XRD patterns of Pt/*x*LA catalysts calcined in air at 573 K and reduced at 923 K are shown in Fig. 1B. No modification in the intensity of XRD patterns of the *x*LA supports (not shown) is observed when compared with Pt/*x*LA catalysts. The XRD analysis results indicate that for La_2O_3 contents ≥6 wt.%, the catalysts exhibit a γ-Al_2O_3 structure (2θ = 33.6°, 37.5°, 39.4°, 45–46° and 67.4°). On the other hand, Pt/Al_2O_3 and Pt/*x*LA catalysts with La_2O_3 loadings lower than 6 wt.% exhibit a mixture of γ- and θ-Al_2O_3 phases [24]. In addition, the intensities of peaks decrease with the increase of La_2O_3 content. XRD reflections characteristic of crystalline La_2O_3 and Pt oxide (2θ = 39.9°) were not detected for any sample. This suggests that Pt and La are both well dispersed.

3.3. Thermogravimetric analysis

TGA and DTGA curves of xerogels are shown in Fig. 2. The TGA profiles of xerogel containing only Al are similar to previously described boehmite [23]. These curves show four regions of weight loss. The first region is at room temperature (ca. 400 K) and it can be assigned to desorption of physically bonded water. The second region is between 430 and 600 K and it is usually related to desorption of water chemically bonded onto the solid surface. The third region is between 600 and 780 K and it corresponds to the

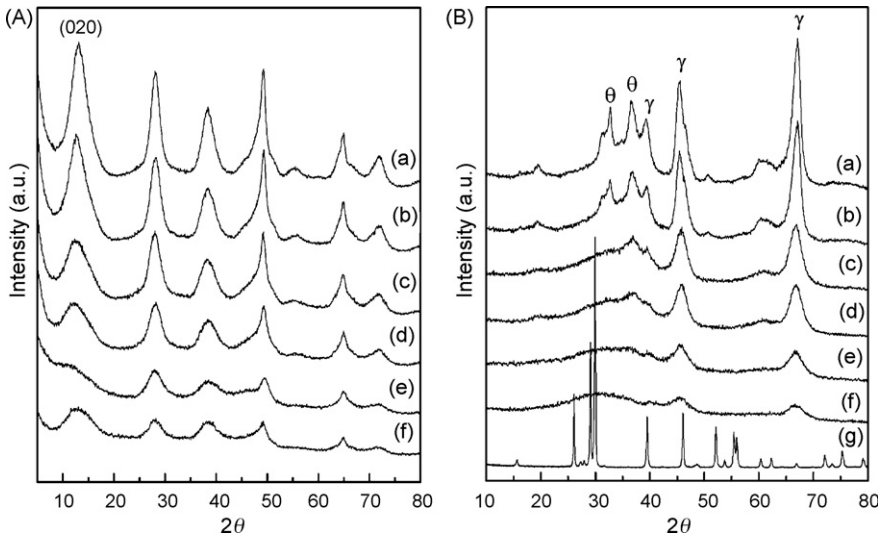

Fig. 1. XRD patterns of the *x*LA xerogels (A) and 0.5Pt/*x*LA catalysts calcined at 573 K and reduced at 923 K (B) with La-content: 0 (a); 1 (b); 3 (c); 6 (d); 12 (e); 20 (f) wt.% La_2O_3 and 0.5Pt/L (g).

dehydroxylation of the boehmite structure to γ-Al_2O_3. Finally, the fourth region, which is detected above 780 K, is correlated to the dehydration of mixed oxides and further transition of Al_2O_3 phases. TGA and DTGA curves for La-containing samples are similar for various La-contents. The increase of La_2O_3 content causes a slightly increased weight loss in the region ca. 430–600 K, corresponding to desorption of chemically bonded water.

3.4. Textural properties

The changes in surface area (S_{BET}), total pore volume (V_p) and average pore diameter (D_p) of *x*LA xerogels, *x*LA supports and Pt/*x*LA catalysts can be observed in Table 1. According to these results, the S_{BET} of *x*LA xerogels exhibited a maximum at 3 wt.% La_2O_3, and decreased for higher La_2O_3 contents. For instance, S_{BET} dropped from 288 $m^2\ g^{-1}$ (for 3 wt.% of La_2O_3) to 86 $m^2\ g^{-1}$ (for 20 wt.% of La_2O_3). The same effect was observed for V_p and D_p. For all *x*LA supports, the addition of small quantities of La_2O_3 led to accentuated decrease of S_{BET}, V_p and D_p (S_{BET} decreases from 325 $m^2\ g^{-1}$ to 190 $m^2\ g^{-1}$). However, no significant modification was found in S_{BET} and D_p of supports with La_2O_3 contents ranging from 3 to 20 wt.%. On the other hand, pore volumes present a continuous decrease with higher amounts of La_2O_3. Comparing Pt/*x*LA catalysts with the corresponding supports, there is a significant decrease in S_{BET} and little changes in V_p and D_p. This suggests that during the impregnation procedures there is some dissolution and precipitation of oxides with blockage of smaller pores [16].

3.5. Temperature-programmed reduction

Fig. 3 displays H_2 uptakes as a function of temperature for calcined Pt/*x*LA samples. It is well known from literature data that different Pt-(O, Cl) species may be formed on the surface during the thermal treatment of Al_2O_3 impregnated with a solution of H_2PtCl_6 [25]. For instance, at 390 K, $PtCl_6^{-2}$ species are found on the γ-Al_2O_3 surface, but at 573 K, there are $[Pt^{IV}(OH)_4Cl_2]_s$-type species. At higher temperatures, around 773 K $[Pt^{IV}O_xCl_y]_s$ species can be identified. Therefore, it is reasonable to suggest that these oxychlorinated species were also formed in Pt/*x*LA since they were treated at 573 K.

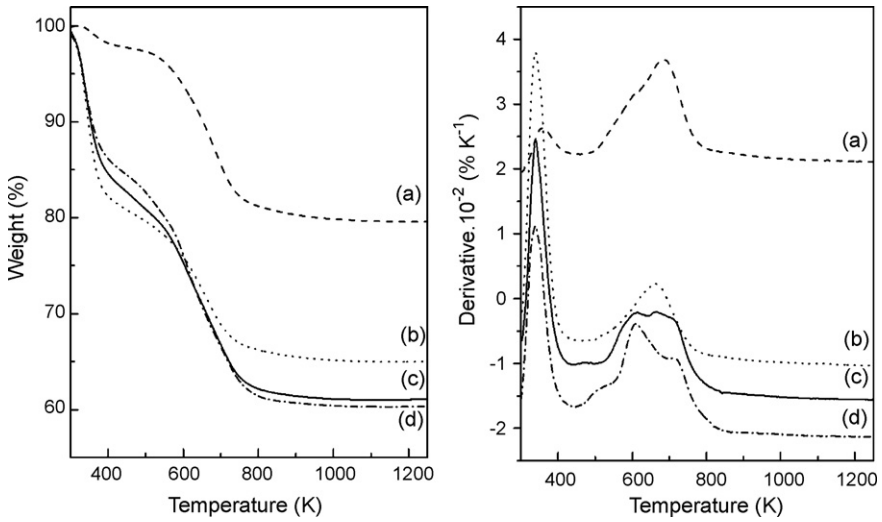

Fig. 2. TGA (A) and DTGA (B) curves of *x*LA xerogels with various La_2O_3 contents: 0 (a); 1 (b); 12 (c); and 20 wt.% La_2O_3 (d).

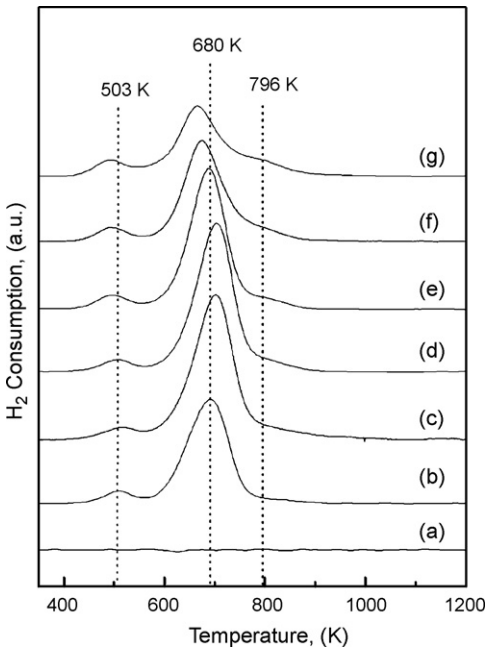

Fig. 3. TPR patterns of Pt/*x*LA catalysts with various La_2O_3 contents: 0 (b); 1 (c); 3 (d); 6 (e); 12 (f); 20 (g) wt.% of La_2O_3 calcined at 573 K and 12LA support (a) calcined at 1223 K.

TPR profiles for Pt/A samples reveal a main peak at 680 K and a minor one at 503 K. The latter can be attributed to the reduction of $[Pt^{IV}(OH)_4Cl_2]_s$ species adsorbed on γ-Al_2O_3 [25]. According to thermal treatment of sample, the main reduction peak should be due to $[Pt^{IV}O_xCl_y]_s$ species, around 520 K. However, for Pt/A (Fig. 3b) this main peak is shifted to higher temperatures, around 680 K. H_2-consumption peaks at high temperatures (652 K) were previously assigned to oxychlorinated species in a two-dimensional phase with strong interaction with alumina [26].

H_2-consumption profiles for Pt/*x*LA catalysts are similar to that obtained for Pt/A. Nevertheless, the temperatures of minor and main peaks are lower for samples with increasing La_2O_3 contents (Fig. 3). In addition, the shoulder around 796 K becames more pronounced with the increase of La_2O_3 loadings. This shoulder could be associated to the reduction of a Pt species with stronger interaction with La_2O_3. For the TPR of 12LA support, the partial reduction of lanthana is not visible.

3.6. ^{27}Al MAS NMR spectroscopy

The ^{27}Al MAS NMR spectra of *x*LA xerogels (Fig. 4) show that the main resonance around 8.0 ppm corresponds to Al(III) ions in AlO_6 sites [27,28] and a resonance around 60 ppm is characteristic of AlO_4 sites, indicating the formation of small quantity of amorphous lanthanum aluminates. Three resonances, around 8.5, 50 and 67 ppm (Fig. 5), are ascribed to hexa-, penta- and four-coordinated Al(III) sites, respectively [29]. These Al(III) sites are typically found in transitional aluminas, while supports with low La-contents apparently show a decreasing number of sites referred to penta-coordinated Al(III) with the increase of calcination temperatures. XRD patterns of *x*LA supports with low La_2O_3 contents indicate the formation of δ- and θ-Al_2O_3 with increasing calcination temperatures (Fig. 1B). On the other hand, the supports with high La_2O_3 loadings show a stable distribution of Al(III) sites with different coordination, with increasing temperatures (Fig. 5). ^{27}Al MAS NMR spectra of Pt/*x*LA catalysts (not presented) are similar to the corresponding *x*LA supports calcined at 1223 K.

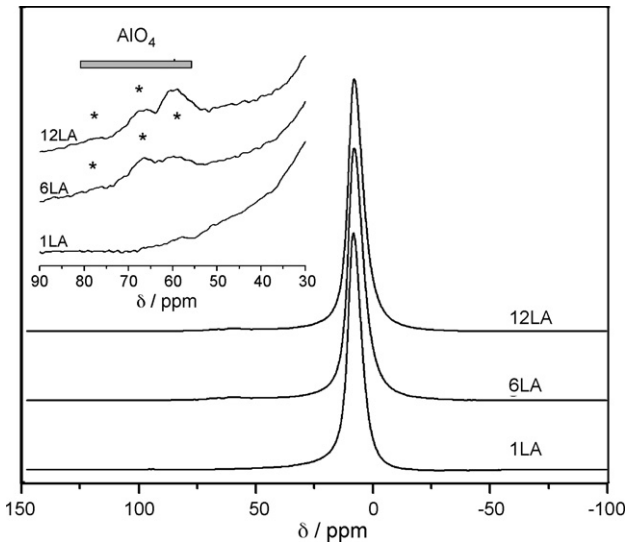

Fig. 4. ^{27}Al MAS NMR spectra of 1LA, 6LA and 12LA xerogels. The inset shows in detail the resonances in the 90–30 ppm range.

3.7. FTIR spectra of adsorbed CO

The IR spectra of CO temperature-programmed desorption of Pt/*x*LA catalysts, in the 1800–1000 cm^{-1} range, are shown in Fig. 6. The Pt/A sample exhibits bands around 1678, 1474, 1403, 1380, 1330, 1295 and 1010 cm^{-1} (Fig. 6A). These bands have been attributed to the reactive adsorption of CO, which usually yields carbonate species (CO_3^{2-}), bicarbonates (HCO_3^-), carboxylates (COO^-) and formate species ($HCOO^-$) [29–31]. The IR spectrum of adsorbed CO on Pt/A catalyst at a temperature lower than 473 K (not shown) present bands at 2967 and 2881 cm^{-1}, characteristic of formate species ($HCOO_{ads}$), assigned to νCH. As proposed by Olympiou et al. [32], formate species could be formed at the periphery of Pt–alumina by spillover of adsorbed CO from Pt and reaction with an –OH from the alumina support. The addition of La(III) caused a shift of the IR band at 1678 cm^{-1} observed for Pt/A catalyst to lower frequencies. For instance, the Pt/12LA catalyst exhibits a band at 1624 cm^{-1}. Although there are reports in the literature about the formation of carbonates after adsorption of CO on La_2O_3 pretreated under vacuum at 973 K (band around 1396 cm^{-1}) [33], these species are suppressed by the increase of La_2O_3 contents in Pt/*x*LA catalysts.

TPD-CO for Pt/A (Fig. 6A) reveals that the species adsorbed at 298 K are reactive and form species with IR bands at 1575 and 1474 cm^{-1}. These species have higher thermal stability and they are decomposed only at temperatures above 573 K. The assignment of these bands is not obvious and the absence of bands at 2967 and 2881 cm^{-1} in the spectra at temperatures ≥473 K excludes the formation of formates species ($HCOO_{ads}$). However, these bands can be attributed to monodentate carbonates [34], which could be formed by reaction of formates with an adjacent –OH group [32]. These species are suppressed by increasing La_2O_3 loadings in the mixed oxides, since they are poorly detected in Pt/*x*LA catalysts with La_2O_3 contents above 6 wt.%. This indicates that the γ-Al_2O_3 surface is significantly modified at higher La_2O_3 contents.

The IR spectra of CO adsorbed on Pt/*x*LA, in the 2200–1700 cm^{-1} range, are displayed in Fig. 7. Pt/A catalyst presents one main band at 2063 cm^{-1} with a shoulder at 2076 cm^{-1} (Fig. 7a). According to the literatures [35–37], these bands at the higher frequency region (around 2060 cm^{-1}) can be attributed to CO linearly bonded to one Pt atom. The shoulder at 2076 cm^{-1} could be assigned to linear CO

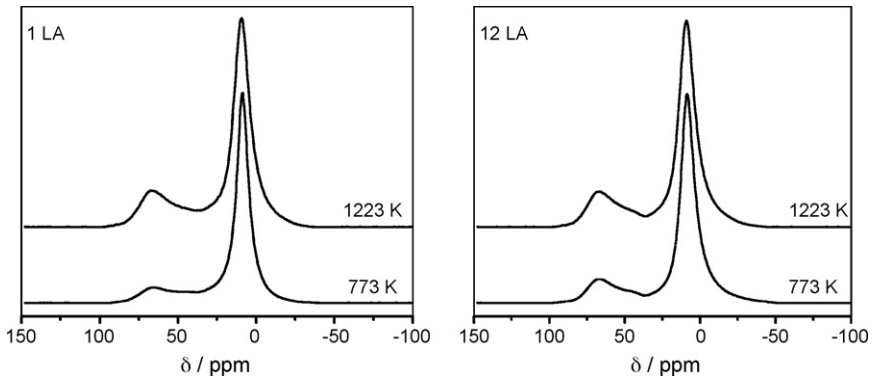

Fig. 5. ^{27}Al MAS NMR spectra of 1LA (left) and 12LA (right) supports calcined at 773 or 1223 K.

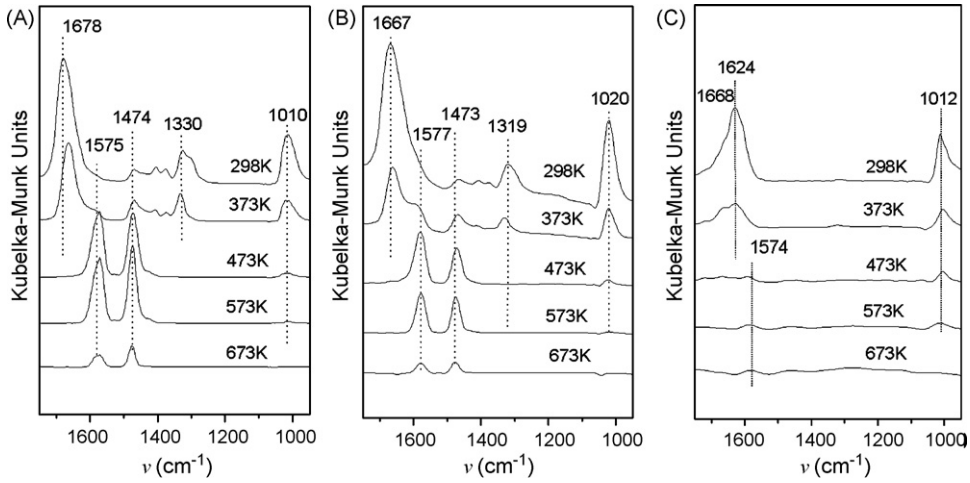

Fig. 6. TPD-CO adsorbed on (A) Pt/A; (B) Pt/1LA and (C) Pt/12LA catalysts. The samples were calcined at 573 K and reduced under H_2 at 923 K, the spectra were taken after CO saturation of the surface of the catalysts at 298 K and P_{CO} = 20 Torr.

species adsorbed on platinum atoms existing in arrays, interacting with the surface of alumina [38]. Pt/1LA catalyst (Fig. 7b) exhibits one additional broad band in the lower frequency region around 1842 cm^{-1}, probably being CO bonded to two surface Pt atoms (bridged species) [35–38]. The increase of La_2O_3 content causes the main band at 2063 cm^{-1} to shift slightly to higher frequency. For catalysts with high La_2O_3 contents (Pt/12LA) both the intensity of the main band and the full width at half-maximum (FWHM) decrease significantly.

3.8. X-ray photoelectron spectroscopy

Binding energy (BE) values of Pt $4d_{5/2}$, La $3d_{5/2}$, Al 2p and O 1s core electron levels for oxidized and reduced Pt/*x*LA catalyst are summarized in Table 2. The Pt 4f line overlapps with Al the 2p and it is not analyzed. BE values of Pt $4d_{5/2}$ are 315.3 ± 0.2 eV for oxidized Pt/*x*LA samples. Similar results have been reported for Pt supported on Al_2O_3 modified with La [26]. For reduced Pt/*x*LA samples, BE values are 313.8 ± 0.2 eV. Typical BE for Pt(II) and Pt(IV) in Pt oxide are 315.3 and 317.0 eV, respectively [39,40]. Comparing BE values of Pt $4d_{5/2}$ obtained for oxidized Pt/*x*LA samples in this study (Table 2) to those from the literature, it may be concluded that these values are close to the ones reported for Pt(II) sites. BE values of Pt $4d_{5/2}$ of reduced Pt/*x*LA catalysts are slightly higher than the values reported for Pt^0 (313.5 eV) [39,40]. This suggests that Pt maintains a δ^+ character in Pt/*x*LA catalysts. Pt/Al + La ratios decrease with the increase of La_2O_3 content (Table 2).

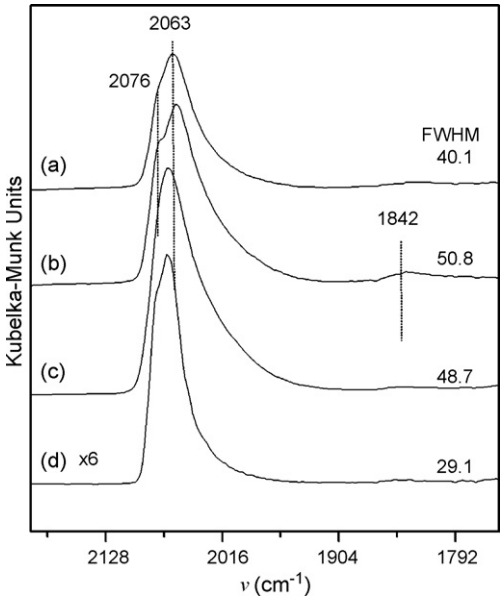

Fig. 7. FTIR spectra of adsorbed CO on Pt/*x*LA catalysts calcined at 573 K and reduced under H_2 at 923 K: Pt/A (a); 1 (b); 6 (c) and 12 (d) wt.% of La_2O_3.

Table 2
XPS parameters of oxidized and reduced Pt/*x*LA catalysts

Catalysts	BE (eV)								
	O 1s		Al 2p		La $3d_{5/2}$		Pt $4d_{5/2}$		Pt/Al + La
	Oxidation[a]	Reduction[b]	Oxidation[a]	Reduction[b]	Oxidation[a]	Reduction[b]	Oxidation[a]	Reduction[b]	Oxidation[a]
Pt/A	531.4	531.3	74.2	74.1	–	–	315.1	314.0	0.005
Pt/L	531.4	531.1	–	–	835.0	835.0	316.0	315.0	0.035
Pt/1LA	531.4	530.2	74.1	73.3	835.2	834.4	315.4	313.6	0.005
Pt/6LA	531.3	529.8	74.2	73.0	835.4	834.1	315.5	313.9	0.004
Pt/12LA	531.3	529.8	74.4	72.9	835.3	834.2	315.2	314.0	0.004

[a] Samples treated in air at 573 K.
[b] Catalysts reduced at 923 K.

BE values of La $3d_{5/2}$ are 835.2 ± 0.2 eV for oxidized Pt/*x*LA samples. However, for reduced samples there is a decrease in these BE values (834.2 ± 0.2 eV). The values for oxidized Pt/*x*LA samples are similar to those reported for $LaAlO_3$ (835.7 eV), $La_2(CO_3)_3$ (835.5 eV) and $La(OH)_3$ (835.9 eV) [41,42]. BE values of La $3d_{5/2}$ for reduced catalysts are close to the ones reported for La_2O_3 (834.9 eV) [42]. On the other hand, BE values of O 1s are around 531.4 eV for oxidized Pt/*x*LA samples, which is characteristic of OH^- and CO_3^{2-} species. For reduced Pt/A catalyst, the BE value of O 1s is also 531.4 eV. However, the increase of La_2O_3 content shifts this BE to lower values (529.8 eV for Pt/12LA) which is characteristic of O^{2-}.

BE values of Al 2p are around 74.2 ± 0.2 eV for oxidized Pt/LA samples, which are characteristic of Al(III). Interestingly, the BE values of Al 2p for reduced Pt/A is 74.1 eV and this value decreases with increasing La_2O_3 content, reaching 72.9 eV for Pt/12LA catalysts. The BE value of Al 2p in Pt/12LA sample is close to the one reported for Al^0 (73.0 eV). These results, coupled with BE of Pt $4d_{5/2}$, that are slightly higher than the ones usually described for Pt^0, suggest that there is a strong interaction between Pt and $(La, Al)_2O_3$ in reduced Pt/*x*LA catalysts. The decreasing BE values observed for Al 2p in comparison to the ones of La $3d_{5/2}$ may be caused by two major effects. One of them is the higher polarizing effect of Al(III) compared to La(III), since Al(III) (53 and 67.5 ppm in four- and six- coordinated sites, respectively) is much smaller than La(III) (1117.2 pm in six-coordinated sites). The second effect is the possible presence of deficiently coordinated La^{3+} ions on the surface of Pt/*x*LA samples reduced at high temperatures [43]. Both effects can lead to a strong interaction between Pt nanoparticles and the mixed oxide support, causing a more noticeable decline in the BE values of Al 2p than La $3d_{5/2}$.

3.9. Catalytic results

Arrhenius plots for steam reforming of methane using Pt/*x*LA catalysts are presented in Fig. 8 and the corresponding apparent activation energies (E_a^{app}) are shown in Table 3. The E_a^{app} for all Pt/*x*LA catalysts are 71 ± 3 kJ mol^{-1} and a higher value is obtained for Pt/L catalyst. This agrees with the values previously reported for steam reforming of methane [1,2]. Interestingly, although La_2O_3-containing catalysts show similar values of E_a^{app}, CH_4 turnover rates (TOF_{CH_4}) become higher with increasing La_2O_3 contents. Similar behavior was previously described for steam reforming of methane on Pd/*x*CeO_2–Al_2O_3 catalysts [3]. The TOF_{CH_4} of Pt/12LA catalyst is about four times higher than the value found for the Pt/A catalyst. Although the number of Pt sites decrease with the increase of La_2O_3 content, the higher TOF_{CH_4} values are a consequence of the enhanced specific rate for steam reforming of methane (r_{CH_4}). The maximum value of r_{CH_4} is found for the Pt/12LA catalyst.

Results of methane conversion (X_{CH_4}) and selectivities to H_2, CO and CO_2 with time on stream during partial oxidation of methane at 1073 K are presented in Fig. 9. Unpromoted Pt/A deactivates significantly during the first 10 h on stream, while Pt/*x*LA catalysts demonstrate only a slight deactivation. Similar to what was observed for steam reforming of methane, Pt/12LA presented the highest activity for partial oxidation of methane.

3.10. Transmission electronic microscopy

Fig. 10 shows TEM images of fresh Pt/A and Pt/12LA catalysts after reduction in H_2 at 923 K. For both samples, TEM images highlight the presence of well-dispersed Pt nanoparticles. Pt/A catalyst presents particles with typical sizes about 5 nm whereas, in Pt/12LA, a population of smaller particles is observed. TEM analyses of Pt/A and Pt/12LA catalysts after a partial oxidation of methane reaction (1073 K and 24 h) exhibit no significant particle aggregation but only the presence of a very few larger particles, of about 10–20 nm in size (data not shown). However, Fig. 11 reveals a Pt particle in Pt/A catalyst where a carbon graphitic layer deposited on its surface is visible. This carbon deposition was not observed for the Pt/12LA catalyst.

4. Discussion

4.1. Effect of La_2O_3 content on the characteristics of Pt/xLA catalysts

Non-calcined xerogels *x*LA containing more than 6 wt.% of La_2O_3 exhibit a significant decrease in the specific surface area and pore volume with the increase of La_2O_3 content (Table 1). This can also be correlated with a decrease of apparent boehmite crystallite size calculated from XRD. The ^{27}Al MAS NMR spectra of *x*LA xerogels show the presence of a resonance around 60 ppm,

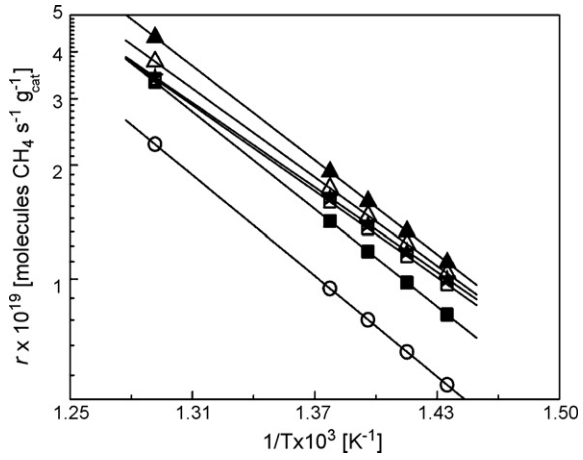

Fig. 8. Arrhenius plot for steam reforming of methane over catalysts with different La_2O_3 loadings: 0 wt.% (■), 1 wt.% (□), 6 wt.% (△), 12 wt.% (▲), 20 wt.% (★), Pt/L (○).

Table 3
Apparent activation energies and TOF_{CH_4} for steam reforming of methane at 773 K

Catalyst	$r_{dehydrogenation} \times 10^{-5}$ (mol s^{-1} g_{cat}^{-1})[a]	Apparent Pt dispersion	$r_{CH_4} \times 10^{-5}$ (mol s^{-1} g_{cat}^{-1})	E_a^{app} (kJ mol^{-1})	TOF (s^{-1})
Pt/A	7.13	0.76	5.52	76.4	2.7
Pt/L	1.20	0.15	3.77	81.8	9.8
Pt/1LA	5.41	0.57	5.62	69.5	3.8
Pt/6LA	4.05	0.43	6.25	70.4	5.6
Pt/12LA	2.25	0.34	7.26	70.3	11.8
Pt/20LA	1.93	0.24	5.46	72.4	8.8

[a] Rate of cyclohexane dehydrogenation at 543 K.

characteristic of AlO_4 sites (Fig. 4). This indicates the formation of amorphous lanthanum aluminates during the sol–gel synthesis of these materials. On the other hand, the ^{27}Al MAS NMR spectrum of the Al_2O_3 support calcined at low temperature (773 K) revealed resonances around 8.5, 50 and 67 ppm (Fig. 5), typically found in low-temperature transition aluminas [24]. In fact, the XRD pattern of this sample is characteristic of γ-Al_2O_3. Al_2O_3 calcined at a high temperature (1223 K) shows predominantly resonances around 8.5 and 67 ppm (Fig. 5), and its XRD pattern indicates the crystallization of θ-Al_2O_3. Alternatively, *x*LA samples calcined at high temperature (1223 K) present ^{27}Al MAS NMR spectra similar to that obtained for γ-Al_2O_3 calcined at lower temperature (773 K). This indicates that the structure of Al_2O_3 is thermally stabilized by the presence of La(III) as suggested by other authors [44]. In this case, La would be in interstitial positions of the transition alumina lattice.

FTIR spectra of CO adsorption and desorption on *x*LA mixed oxides (Fig. 6) show that it was not possible to detect the presence of formate species ($HCOO_{ads}$) or of monodentate carbonate species with IR bands around 1575 and 1474 cm^{-1} on the surface of La-containing supports. Therefore, it is expected that the Al_2O_3 surface is covered by La_2O_3 when the lanthana content in the support is above 6 wt.%. The main band of adsorbed CO on Pt/*x*LA catalysts is around 2060 cm^{-1} for various La_2O_3 contents (Fig. 7). However, this band exhibits a broadening on the low frequency side. For Pt/*x*LA catalysts with $x \leq 6$ wt.% of La_2O_3, the FWHM is about 40–50 cm^{-1}. This main band becomes more symmetric, with lower FWHM (29 cm^{-1}) and lower intensity for the Pt/12LA sample. It is important to point out that (i) smaller Pt particles have lower coordination numbers and higher electron densities, (ii) back-donation of 5d electrons of Pt into the 2π antibonding orbital of the C≡O molecule increases with decreasing Pt particle sizes and, consequently, (iii) the decrease of Pt particle size leads to a decrease in C≡O bond strength and to a shift in the position of the IR bands to lower frequencies. Therefore, the broad band at 1842 cm^{-1} for Pt/*x*LA catalysts with $x \leq 6$ wt.% can be correlated to the presence of smaller Pt particles with higher electron densities, which are accessible to CO adsorption. The lower FWHM (29 cm^{-1}) for Pt/12LA catalyst suggests a higher uniformity of electron densities of the Pt sites. The bands at different positions referring to CO adsorbed in the linear form reflect the presence of Pt sites with different electron densities. Two factors should be considered in

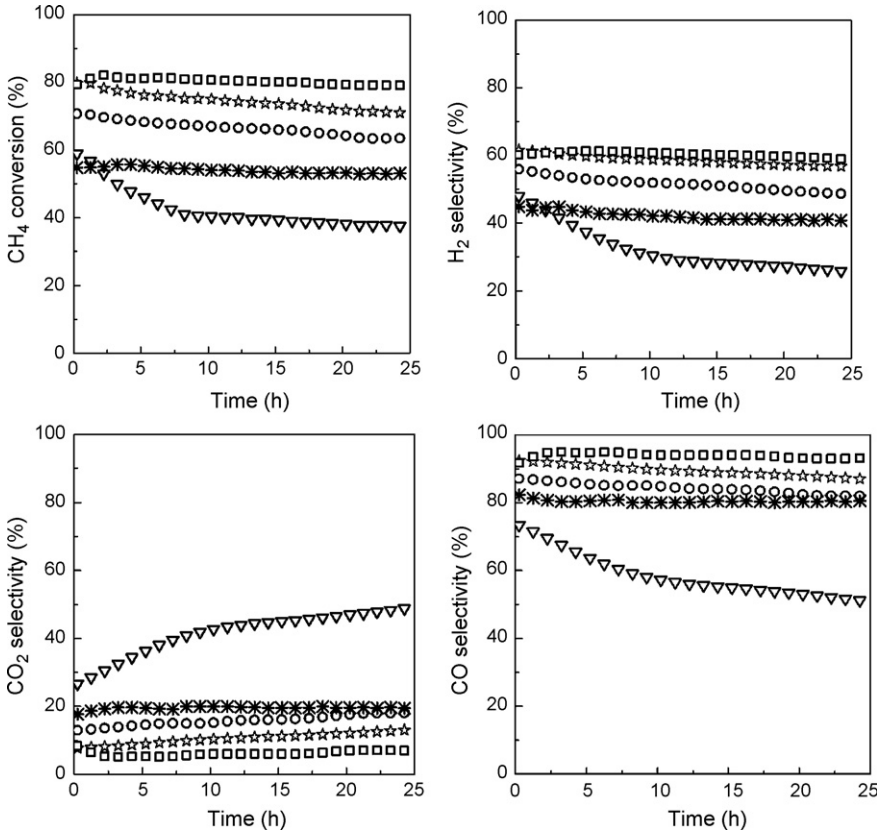

Fig. 9. Partial oxidation of CH_4 at 1073 K: CH_4 conversion and selectivities to H_2, CO and CO_2 over Pt/*x*LA catalysts with various La_2O_3 contents: 0 (▽); 1 (○); 6 (✳); 12 (□) and 20 wt.% of La_2O_3 (✳).

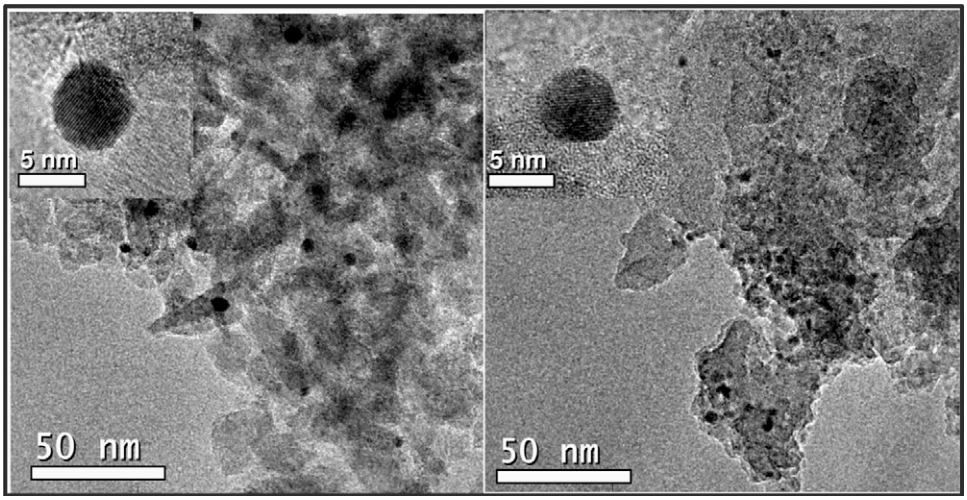

Fig. 10. TEM images of fresh Pt/A (left) and Pt/12LA (right) catalysts after reduction at 923 K. The insets present HRTEM images, showing the lattice fringes corresponding to the (1 1 1) planes of Pt.

the interpretation of the bands related to Pt species (a shoulder around 2076 cm^{-1} and a main band around 2060 cm^{-1}): (i) the presence of Cl^- ions interacting with Pt, which can act as an electron withdrawing ligand, decreases the electron density of the Pt 5d orbital and shifts the CO band to higher frequencies; (ii) the morphology of the Pt particle can result in different defects on the surface. The presence of Pt step sites, with lower Pt coordination numbers than terrace sites, can shift the CO band to lower frequency. However, the higher frequency band, at 2060 cm^{-1}, is characteristic of CO adsorption on terrace sites, according to Tanaka and White [45]. It is interesting to note that the band at 1817 cm^{-1}, assigned to bridge-bonded CO species (which are geometrically favored on terrace sites), is not observed for Pt/12LA. Nevertheless, the FWHM (29 cm^{-1}) of the band at 2060 cm^{-1} and the lower intensity of the CO band observed for Pt/12LA catalyst, as well as a lower cyclohexane dehydrogenation reaction rate, should not be interpreted as a simple effect of lower Pt dispersion in catalysts with high La_2O_3 contents. Therefore, to obtain an insight into the effect of La_2O_3 content on the properties of Pt particles, TEM results must also be considered. TEM images of Pt/A and Pt/12LA catalysts (Fig. 10) show average Pt particle sizes around 5 and 4 nm, respectively. This suggests higher Pt dispersion for catalysts with high La_2O_3 content (Pt/12LA). Then, it is reasonable to propose that the decrease of accessibility to cyclohexane and to CO adsorption to metallic sites is an effect of partial coverage of Pt particles by LaO_x–Pt species. It means that the smaller Pt particles in the Pt/12LA catalyst are favoring the interaction of such LaO_x species, suppressing the accessibility of Pt sites to cyclohexane dehydrogenation and to CO adsorption. The suppression of adsorbed CO in the bridge form may be due to a geometric effect. The partial coverage of a noble metal by La_2O_3 is not surprising and it has been proposed by Fleisch et al. for Pd/La_2O_3 catalysts [42]. In this study, these authors suggested that La_2O_3 is partially reduced during H_2 treatment at 573 K to form $LaPd_xO$ species.

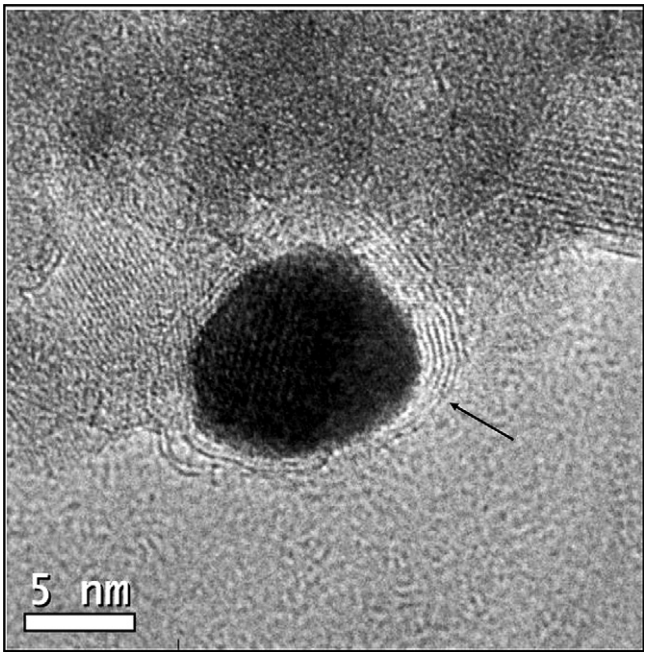

Fig. 11. TEM image of a Pt nanoparticle in the Pt/A catalyst after partial oxidation of methane. The arrow points to the presence of a deposit of a graphitic layer on its surface.

4.2. Effect of La_2O_3 content on the activity of Pt/xLA catalysts for steam reforming of methane

The value of E_a^{app} (71 ± 3 $kJmol^{-1}$) obtained for the steam reforming of CH_4 on Pt/*x*LA catalysts suggests that the properties of the active Pt sites are not significantly different for various La_2O_3 contents. However, the IR spectra of adsorbed CO show the presence of a fraction of Pt sites with higher electron density for catalysts with low La_2O_3 contents. Therefore, it would be reasonable to assume that the TOF_{CH_4} of these particles would be higher than in catalysts containing Pt sites with lower electron densities. In order to understand these activity results, a mechanism of reforming of CH_4 similar to the one reported in an earlier paper for steam reforming of methane on Pd/CeO_2/Al_2O_3 catalysts, should be considered [3]. This mechanism was originally proposed by Wei and Iglesia [1,2] and it states that CH_4 decomposes to form chemisorbed carbon (C*) via sequential elementary H-abstraction steps. This is a structure-sensitive reaction and it is the rate-limiting step [46]. C^* on the surface can be formed by either CH_4 activation [1,47] or by CO decomposition. The active C^* can be removed by reaction with surface oxygen (O^*) to produce CO. Therefore, the amount of C^* on the surface depends on its stability and on the amount of O^* available for the reaction $C^* + O^* \leftrightarrow CO$. According to the literature [48], the stability of

C^* on the surface is higher for Pt sites with high electron densities. The IR spectra of adsorbed CO suggest the presence of a larger fraction of Pt particles with higher electron density in Pt/*x*LA catalysts with lower La_2O_3 contents, which are more susceptible to C^* accumulation.

On the other hand, for higher La_2O_3 contents, the TEM results reveal a decrease of Pt particle size. In this case, the IR spectra show a suppression of CO adsorption and XPS data demonstrate a decrease of Pt/Al + La ratio. These results indicate that Pt particles may be partially covered by Al[LaO_x] species. Similar to results previously reported for Pd/La_2O_3 [42], Al[$LaPt_xO$] species on Pt may be oxidized by H_2O or CO_2 or through oxygen transfer from (OH/H) species located on the surface of the support, as suggested by Olympiou et al. [32]. These oxidized Al[$LaPt_xO$] species may form others species such as La_2O_3, $La(OH)_3$ and/or LaO(OH) on the Pt surface. These new species could be reduced by C^* deposited on the Pt surface to restore Al[$LaPt_xO$] species and the active Pt sites that were blocked by C^*. Consequently, the partial blocking of Pt sites by carbon should lead to a decrease of the TOF_{CH_4} value, calculated from the number of Pt sites accessible to cyclohexane dehydrogenation. Nevertheless, the specific rate for steam reforming of CH_4 increases with the La_2O_3 content, reaching a maximum at 12 wt.%. This indicates that very active Pt sites became accessible to CH_4 with the increase of La_2O_3 loading and compensate for the partial coverage of Pt by LaO_x species.

4.3. Effect of La_2O_3 contents on the stability of Pt/xLA catalysts for partial oxidation of methane

At least two effects of La_2O_3 on stability can be identified: (i) suppression of carbon deposition and (ii) inhibition of the sintering process of Pt particles. A two-step mechanism has been proposed for the partial oxidation of methane, consisting of total oxidation of methane and reforming steps of the unreacted CH_4 with steam and CO_2 [49]. Considering that methane oxidation is faster than the reforming reactions [4,49], it is expected that, at the reactor entrance, there is an oxygen-rich region where the oxidation predominantly occurs. Closer to the reactor exit, the reforming reactions would prevail due to a more oxygen-deficient flow. Therefore, the atmosphere will be distinct and the stability of Pt catalysts will be different in these two regions. In the region where reforming reactions are predominant, the main mechanism of deactivation would be carbon deposition. The deposition of carbon on Pt/A catalyst can be due to the low ability of this catalyst to gasify carbon. The presence of La_2O_3 increases the ability of the catalyst to remove carbon deposits, by activating H_2O or CO_2 on $LaPt_xO$-like sites over the Pt particle and transferring the O^* species to C^*. In the region of oxidation reactions, the main mechanism of deactivation might be the growing of Pt particles. Since the sublimation energy is higher for Pt–Pt than for PtO_2, as demonstrated by Wynblat [50], PtO_2 serves as an intermediate to inter-cluster transport by the vapor phase and to surface diffusion. In this case, the partial coverage of the Pt particle by La_2O_3 under an oxidizing atmosphere can promote the Pt–O–La interaction, similar to the sintering inhibition mechanism proposed by Nagai et al. [5] for a Pt/ceria-based oxide catalyst. A Pt–O–La interaction can act as an anchor and inhibit the transport of PtO_2 inter-clusters. On the other hand, the BE of O 1s has the same value of 531.4 eV for both Pt/A and Pt/L oxidized catalysts. XPS results of oxidized Pt/*x*LA catalysts show the presence of Pt(II) sites. Therefore, the higher stability of Pt/*x*LA catalysts with higher La_2O_3 content in the partial oxidation of methane cannot be related only to the increase of Pt–O–La interactions. Two other effects can be considered: first, Pt/*x*LA catalysts with high La_2O_3 contents show partial coverage of Pt particles by LaO_x. Obviously, this interface can result in higher Pt–O–La interaction in comparison to Pt–O–Al in Pt/A catalyst. Although TEM data suggest a decrease of Pt particle sizes with the increase of La_2O_3 content, XPS results demonstrate a decrease of Pt/Al + La ratio in oxidized samples, indicating an increase of Pt–O–La species. This interaction may stabilize Pt in an oxidized state and can act as a barrier to inter-cluster transport by vapor phase diffusion. Second, ^{27}Al MAS NMR and XRD results reveal higher stabilities of the γ-Al_2O_3 structure for La_2O_3-containing catalysts and it is reasonable that the higher stability of the support helps to decrease the mobility and coalescence of Pt particles.

5. Conclusions

The results allow the following conclusions:

- La_2O_3–Al_2O_3 xerogels obtained by a sol–gel synthesis have a pseudo-boehmite structure. The presence of Al(III) in an amorphous phase increases for higher La_2O_3 contents. ^{27}Al MAS NMR spectra of La_2O_3–Al_2O_3 mixed oxides show Al(III) ions distributed in AlO_4, AlO_5 and AlO_6, characteristic of γ-Al_2O_3, which is thermally stabilized by the presence of La(III).
- The reactivity of CO in the adsorption and desorption processes on *x*La_2O_3–Al_2O_3 mixed oxides suggests that the Al_2O_3 surface is covered by La(III) species at La_2O_3 contents above 6 wt.%.
- Pt/A catalyst shows an average Pt particle size around 5 nm. Although there is a decrease in Pt particle size with the increase of La_2O_3 content, Pt particles are partially covered by LaO_x species. As a result, the number of Pt sites for dehydrogenation of cyclohexane decreases with the increase of La_2O_3 loading.
- Pt/*x*La_2O_3–Al_2O_3 catalysts show a maximum of specific activity for steam reforming of methane at 12 wt.% of La_2O_3. The TOF_{CH_4}, calculated from Pt sites accessible to the dehydrogenation of cyclohexane, increases with the increase in La_2O_3 content. The IR band of CO adsorbed on Pt is strongly suppressed with the increase of La_2O_3 loading and reflects a narrow electronic density distribution of Pt sites. Pt sites in Pt/*x*La_2O_3–Al_2O_3 catalysts show similar E_a^{app}, although there is an increase of TOF_{CH_4} for steam reforming of methane. This increase is assigned mainly to the ability of $LaPt_xO$-like species on the Pt surface to promote C^* removal and to the increase of CH_4 accessibility to the active sites.
- Pt/12La_2O_3–Al_2O_3 catalyst shows the highest catalytic activity and stability in the partial oxidation of methane. The higher stability of La_2O_3-containing catalysts during partial oxidation of methane cannot be easily connected to the anchoring of Pt particles due to the similarity of the bonding energies of both Al–O–Pt and La–O–Pt.
- All results suggest that the metal–support interface and the nature of the support have important roles in the accessibility and stability of Pt sites.

Acknowledgments

LME-LNLS, Brazil is acknowledged for the use of TEM. The authors are grateful for the financial support of FAPESP (Fundação para o Amparo à Pesquisa do Estado de São Paulo) and CNPq (Conselho Nacional de Desenvolvimento científico e Tecnológico). J. Liberatori assisted in obtaining the TEM images.

References

[1] J. Wei, E. Iglesia, J. Catal. 224 (2004) 370.
[2] J. Wei, E. Iglesia, J. Catal. 225 (2004) 116.
[3] L.S.F. Feio, C.E. Hori, S. Damyanova, F.B. Noronha, W.H. Cassinelli, C.M.P. Marques, J.M.C. Bueno, Appl. Catal. A: Gen. 316 (2007) 107.

[4] A.C.S.F. Santos, S. Damyanova, G.N.R. Teixeira, L.V. Mattos, F.B. Noronha, F.B. Passos, J.M.C. Bueno, Appl. Catal. A: Gen. 290 (2005) 123.
[5] Y. Nagai, T. Hirabayashi, K. Dohmae, N. Takagi, T. Minami, H. Shinjoh, S. Matsumoto, J. Catal. 242 (2006) 103.
[6] S. Irusta, L.M. Cornaglia, E.A. Lombardo, J. Catal. 210 (2002) 7.
[7] Z.L. Zhang, V.A. Tsipouriari, A.M. Efstathiou, X.E. Verykios, J. Catal. 158 (1996) 51.
[8] H.Y. Wang, E. Ruckenstein, Appl. Catal. A: Gen. 204 (2000) 143.
[9] A. Vazquez, T. Lopez, R. Gomez, X. Bokhimi, J. Mol. Catal. A: Chem. 167 (2001) 91.
[10] J. Livage, M. Henry, C. Sanchez, Progr. Solid State Chem. 18 (1988) 259.
[11] C.J. Brinker, G.W. Scherer, Sol–Gel Science, Academic Press, New York, 1989.
[12] J. Livage, Catal. Today 41 (1998) 3.
[13] R. Rinaldi, U. Schuchardt, J. Catal. 227 (2004) 109.
[14] D.J. Suh, T.-J. Park, J.-H. Kim, K.-L. Kim, J. Non-Cryst. Solids 225 (1998) 168.
[15] G. Pecchi, P. Reyes, R. Gomez, T. Lopez, J.L.G. Fierro, Appl. Catal. B Environ. 17 (1998) L7.
[16] A. Barrera, M. Viniegra, P. Bosch, V.H. Lara, S. Fuentes, Appl. Catal. B: Environ. 34 (2001) 97.
[17] J.B. Miller, E.I. Ko, Catal. Today 35 (1997) 269.
[18] R.D. Gonzalez, T. Lopez, R. Gomez, Catal. Today 35 (1997) 293.
[19] H. Kobayashi, K. Tadanaga, T. Minami, J. Mater. Chem. A: Chem. 8 (1998) 1241.
[20] S. Damyanova, J.M.C. Bueno, Appl. Catal. A: Gen. 253 (2003) 135.
[21] A. Vazquez, T. López, R. Gómez, X. Bokimi, A. Morales, O. Navaro, J. Solid State Chem. 128 (1997) 161.
[22] E. Rogemond, N. Essayem, R. Frety, V. Perrichon, M. Primet, F. Mathis, J. Catal. 166 (1997) 229–235.
[23] R. Rinaldi, U. Schuchardt, J. Catal. 236 (2005) 335.
[24] X. Wu, B. Yang, D. Weng, J. Alloys Compd. 376 (2004) 241.
[25] H. Lieske, G. Lietz, H. Spindler, J. Völter, J. Catal. 81 (1983) 8.
[26] R.M. Navarro, M.C. Álvarez-Galván, M. Cruz Sánchez-Sánchez, F. Rosa, J.L.G. Fierro, Appl. Catal. B: Environ. 55 (2005) 229.
[27] J.A. Wang, X. Bokhimi, A. Morales, O. Novaro, T. Lopez, R. Gomez, J. Phys. Chem. B 103 (1999) 299.
[28] R. Rinaldi, F.Y. Fujiwara, U. Schuchardt, Appl. Catal. A: Gen. 315 (2006) 44.
[29] K.I. Hadjiivanov, G.N. Vayssilov, Adv. Catal. 47 (2002) 307.
[30] G. Busca, V. Lorenzelli, Mater. Chem. 7 (1982) 89.
[31] M.A. Babaeva, D.S. Bystrov, A. Yukovalgin, A.A. Tsyganenko, J. Catal. 123 (1990) 396.
[32] G.G. Olympiou, C.M. Kalamaras, C.D. Zeinalipour-Yazdi, A.M. Efstathiou, Catal. Today 127 (2007) 304–318.
[33] A.A. Tsyganenko, J. Lamotte, J.P. Gallas, J.C. Lavalley, J. Phys. Chem. 93 (1989) 4179.
[34] A. Iordan, M.I. Zaki, C. Kappenstein, Phys. Chem. Chem. Phys. 6 (2004) 2502.
[35] M. Primet, J.M. Basset, M.V. Mathieu, M. Prettre, J. Catal. 29 (1973) 213.
[36] R. Barth, R. Pitchai, R.L. Anderson, X.E. Verykios, J. Catal. 116 (1989) 61.
[37] S.D. Jackson, B.M. Glanville, J. Willis, G.D. Mclellan, G. Webb, R.B. Moyes, S. Simpson, P.B. Wells, R. Whyman, J. Catal. 139 (1993) 207.
[38] J. Xu, J.T. Yates, Surf. Sci. 327 (1995) 193.
[39] J.Z. Shyu, K. Otto, Appl. Surf. Sci. 32 (1988) 246.
[40] S.D. Jackson, J. Willis, G.D. Mclellan, G. Webb, M.B.T. Keegan, R.B. Moyes, S. Simpson, P.B. Wells, R. Whyman, J. Catal. 139 (1993) 191.
[41] J.S. Ledford, M. Houalla, A. Proctor, D.M. Hercules, J. Phys. Chem. 93 (1989) 6770.
[42] T.H. Fleisch, R.F. Hicks, A.T. Bell, J. Catal. 87 (1984) 398.
[43] R. Alvero, A. Bernal, I. Carrizosa, J.A. Odriozola, Inorg. Chim. Acta 140 (1987) 45.
[44] K.N.P. Kumar, J. Tranto, J. Kumar, J.E. Engell, J. Mater. Sci. Lett. 15 (1996) 266.
[45] K. Tanaka, J.M. White, J. Catal 79 (1983) 81.
[46] T.V. Choudhary, D.W. Goodman, J. Mol. Catal. A: Chem. 163 (2000) 9.
[47] I. Alstrup, M.T. Tavares, J. Catal. 135 (1992) 147.
[48] H.S. Bengaard, J.K. Norskov, J. Sehested, B.S. Clausen, L.P. Nielsen, A.M. Molenbroek, J.R. Rostrup-Nielsen, J. Catal. 209 (2002) 365.
[49] J.A.C. Ruiz, F.B. Passos, J.M.C. Bueno, E.F. Souza-Aguiar, L.V. Mattos, F.B. Noronha, Appl. Catal. A: Gen. 334 (2008) 259.
[50] P. Wynblatt, Acta Metall. 24 (1976) 1175.